Heating Rate within the Upper Ocean in Relation to Its Bio-Optical State

ANDRÉ MOREL AND DAVID ANTOINE

Laboratoire de Physique et Chimie Marines, Université Pierre et Marie Curie et CNRS, Villefranche sur Mer, France

18 May 1993 and 8 December 1993

ABSTRACT

Solar radiation absorption and local heating within the upper layers of the open ocean are strongly influenced by the abundance of phytoplankton as depicted by the chlorophyll concentration. According to whether this concentration is high or low, the heat deposition occurs within a layer that may vary in thickness from less than 10 m to more than 100 m. A simple parameterization, accounting for this dependence, is developed. It allows the vertical profiles of heating rate to be predicted from the phytoplanktonic pigment concentration, as it can (and will) be remotely detected from space, by using ocean color sensors. This computationally efficient parameterization has been validated in reference to the results of a full spectral model. In the simplified computation, the solar spectrum is partitioned into two domains, below and above the wavelength 0.75 μm. For the infrared waveband, not influenced by biological materials, the irradiance profile is described by a single exponential function. For the ultraviolet and visible (<0.75 μm) band, a bimodal exponential form is adopted. The weights associated with each of these exponential functions, as well as their specific attenuation lengths, are dependent upon pigment concentration. These dependences are explicated through polynomial formulas. The remotely sensed pigment values can thus be readily introduced in numerical models of the mixed layer and of regional upper ocean dynamics or general circulation.

1. Introduction

When modeling locally in a one-dimensional way or at large-scale physical processes occurring within the upper oceanic layer, the heating rate resulting from solar radiation absorption has to be reliably parameterized and assessed. Satellites provide a new avenue by which information relevant to this problem can be gathered at the required space and time scales. Numerical tools have to be prepared in view of assimilating such data into regional and global models. The total incoming solar radiation at the ocean surface can presently be estimated from space (e.g., Gautier et al. 1980; Dedieu et al. 1987; Bishop and Rossow 1991) and the cloud coverage permanently monitored (Rossow and Schiffer 1991). The "bio-optical state" (Smith and Baker 1978) of the upper ocean, and namely its chlorophyll-like pigment content, will be soon continuously determined from space using operational ocean color sensors like the SeaWIFS and its successors. This pigment concentration is the appropriate variable that can be directly used to predict in an accurate way the vertical profile of the heating rate.

At sea level, about half of the solar radiation lies in wavelengths longer than the visible spectral region. The solar infrared (IR) radiation ($\lambda > 0.75$ μm) is rapidly absorbed within the top ~10-cm layer; in contrast, the visible and near-ultraviolet (UV) radiation (the other half) is much more penetrative into oceanic waters. It is also absorbed with varying rates depending essentially, in oceanic case 1 waters, on the pigment content (Morel 1988; Lewis et al. 1990). In these waters the chlorophyllous pigment concentration may span over about three orders of magnitude (between say 0.02 and 20 mg m^{-3}), and in correspondence, the euphotic depth, Z_e, varies between about 120 and 10 m. The euphotic depth is defined as the depth where the downwelling photosynthetically available radiation (PAR) is reduced to 1% of its surface value. By noting that PAR and the visible spectral domain approximately coincide, the euphotic layer is therefore that layer inside which 99% of the visible radiation has been absorbed. The above extreme Z_e values demonstrate how the heated layer can be highly variable in thickness in the open ocean.

The aim of the present work is to develop a computationally efficient, yet accurate, parameterization of the whole solar radiation absorption, as modulated in its visible portion by the algal pigment content within the upper oceanic layers.

2. Background

Several parameterizations of the vertical gradient of downward solar irradiance and thence of the vertical heating profile have been proposed. The simplest form is a single exponentially decreasing function of depth

Corresponding author address: Dr. André Morel, Laboratoire de Physique et Chimie Marines, Université Pierre et Marie Curie et CNRS, BP 08, F 06230 Villefranche sur Mer, France.

(e.g., Denman 1973). A bimodal exponential function (Kraus 1972; Paulson and Simpson 1977) can simultaneously account for the preferential absorption of the red and near-infrared portion of the solar spectrum, and for the slower decay of the most penetrative (visible) component. In the same way Simpson and Dickey (1981) suggested a decomposition into nine spectral bands, each with their specific exponential functions of depth. Raschke (1975) and Woods (1980) considered many bands combined with the absorption coefficients for pure water only. Zaneveld and Spinrad (1980) reproduced the irradiance–depth curve using a combination of an exponential function with an arc tangent function. Calculations of heating rate within highly colored and turbid inland waters were also presented by Kirk (1988).

In Paulson and Simpson (1977) and in Zaneveld et al. (1981), the required parameters (4) were determined for each of the Jerlov's "water types" (1976). Such tunable parameterizations can be operated as far as the water considered may be categorized within the scheme of Jerlov's classification (Simonot and LeTreut 1986). This descriptive classification, however, does not rely on the bio–optical state of the ocean water (the chlorophyll-like pigment content). It rests on the variations in ocean transparency, as they have been observed, without attempting to relate these variations to their very causes, namely, to the presence of pigmented biological materials. Phytoplankton, with their retinue, actually play the dominant role in determining the optical properties of oceanic case 1 waters (Morel and Prieur 1977). Note that the oceanic optical water types (from I to III), as defined by Jerlov, are all included in oceanic case 1 waters, which range from eutrophic (high chlorophyll content) to oligotrophic (extremely low content) waters. The chlorophyll-like pigment concentration (i.e., Chlorophyll *a* plus Phaeophytin a, thereafter denoted C) is the convenient index for quantifying the whole algal (and derivative) material. The spectral coefficients for attenuation of the downwelling visible irradiance can be modeled as continuous functions of C (Morel 1988). In this reference, the in-water heating due to visible (0.4–0.7 μm) radiation has already been assessed in relation to C by considering uniform pigment profiles and 61 wavelengths. If the penetration of PAR must be described in detail when trying to analyze and predict the photosynthetic activity, such a large number of bands conceivably becomes superfluous when dealing with the heating rate. A simpler parameterization is to be developed for incorporation into global models, to be fed with information about the chlorophyll content, as expected from future ocean color sensors.

3. Formulation of the problem

The time rate of radiant energy, E_{abs}, absorbed per unit of volume at a particular depth Z (positive downward) is expressed as [symbols and definitions are those recommended by the International Association for the Physical Sciences of the Ocean (IAPSO); see Morel and Smith (1983)]

$$E_{abs} = a\mathring{E},$$

where a is the absorption coefficient (m^{-1}) and $\mathring{E}$ is the scalar irradiance (W m^{-2}) at the depth in question. The conservation of energy states that this amount is simply the derivative with respect to depth of the downward vector irradiance $\vec{E}$ if the horizontal divergence is negligible, as in a horizontally homogeneous water body. The modulus of $\vec{E}$, also called the "net" downward irradiance, is the difference between the downward irradiance, E_d, and the upward irradiance, E_u, so that

$$a\mathring{E} = -d\vec{E}/dZ = -d(E_d - E_u)/dZ. \quad (1)$$

The vertical attenuation coefficient for any of the irradiances above (E) is defined as

$$K_x = -d[\ln E_x(Z)]/dZ, \quad (2)$$

where $x = d$, u, v, or o according as E_x is E_d, E_u, E, or $\mathring{E}$.

Rather than $\vec{E}$ or $\mathring{E}$, the irradiance that is more commonly determined (and thus modeled) is the downwelling irradiance E_d. Equation (1) can be simply transformed into

$$a\mathring{E} = K_d E_d[1 - R(K_u/K_d)], \quad (3)$$

where R is the reflectance, defined as being the ratio E_u/E_d. The relative importance of the correction represented by the bracketed term is discussed in the appendix. Suffice it to say now that the ratio K_u/K_d never differs significantly from 1 and that R is essentially zero in oceanic waters for the red and infrared domain, so that in this domain Eq. (3) reduces to

$$a\mathring{E} = K_d E_d. \quad (3')$$

In contrast, R is not zero in the visible part of the spectrum and an accurate estimate of E_{abs} must account for the existence of an upward light stream. This is achieved by operating Eq. (1), where the net downward irradiance is obtained through $E_d(1 - R)$, provided that R can be determined (see the appendix).

Neglecting other pathways for absorbed radiant energy (see discussion below), this absorption process essentially results in an instantaneous local increase of heat content and thus in temperature, θ, according to

$$d\theta(Z, t)/dt = E_{abs}(Z, t)/\rho c_p, \quad (4)$$

where ρ is the density ($\sim$1025 kg m^{-3}), c_p the thermal capacity [$\sim$4.17 KJ $(K)^{-1}$ kg^{-1}], and dt = 1 second when E_{abs} is expressed as W m^{-3}.

All the radiometric quantities (the E, K, R, a) are wavelength-dependent even if the argument λ has been omitted in the above equations. The spectral compo-

sition of the incident radiation at the surface, and thereafter its progressive transformation throughout the water column, remain to be examined.

4. Spectral composition of the solar flux at various levels

a. *Solar irradiance at the sea surface*

About 99.5% of extraterrestrial solar radiation falls between $\lambda = 0.25$ and $\lambda = 4.25$ μm (e.g., see Neckel and Labs 1984). Due to atmospheric gases (CO_2 and H_2O mainly) acting as efficient absorbers in the near-IR region, the spectral composition of the solar radiation at the sea surface is deeply modified, and practically no energy (<0.9%) subsists beyond 2.5 μm. Due to N, O, O_2, and O_3 atmospheric absorption, the radiation with $\lambda < 0.3$ μm does not reach the bottom of the atmosphere. As an example, the spectral composition of the incident radiation at the sea surface (Fig. 1) has been computed for a solar zenith angle of 45° by operating the "5S" atmospheric model (Tanré et al. 1979, 1990) with vertically integrated water and ozone contents of 2 g cm^{-2} and 0.35 cm atm, respectively, and with aerosols, of maritime type, corresponding to a visibility of 23 km. For clear skies the relative proportions of IR and shortwave radiation depend in a predictable manner on the solar elevation angle and on atmospheric properties (e.g., Tanré et al. 1979; Iqbal 1983). Under cloudy skies, the proportion of shortwave radiation is relatively reinforced, in a manner that varies according to the cloud cover and liquid water content (e.g., Stephens 1978; Nann and Riordan 1991).

b. *Transmission across the atmosphere–ocean interface*

The downwelling irradiance impinging just above the surface, denoted $E_d(0^+)$, is not totally transmitted through the interface and is reduced immediately below the interface into $E_d(0^-)$, according to

$$E_d(0^-) = E_d(0^+)(1 - \rho_F - \rho_D), \qquad (5)$$

where the sum $(\rho_F + \rho_D)$ constitutes the albedo of the ocean, which includes the Fresnel reflection at the air–water boundary, ρ_F, and the diffuse reflection originating from the upper layers, ρ_D, much smaller than ρ_F (see the appendix).

To the extent that the refractive index of sea water is only a weakly decreasing function of wavelength, the Fresnel reflection term is approximately constant throughout the spectral domain considered; actually it decreases by 20% between 0.3 and 2 μm. Therefore, the spectral composition of the radiation having crossed the interface remains essentially unchanged with respect to that prevailing above. The diffuse reflection term differs from zero in the visible part of the spectrum only, and, in this case, the backscattered flux is wavelength dependent (see the appendix).

c. *In-water propagation and possible partitioning*

1) INFRARED DOMAIN

Compared to that in the near-UV and visible range, the water absorption in the IR domain is so enormously

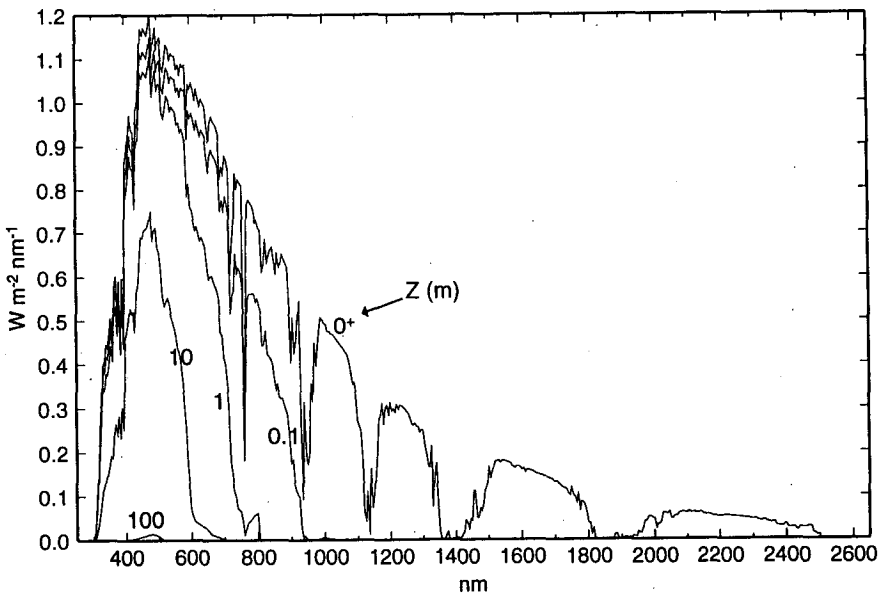

FIG. 1. Computed spectral composition of the downwelling solar irradiance impinging at the surface (0^+) and then propagated to various depths (Z = 0.1, 1, 10, and 100 m). The propagation is computed assuming a chlorophyll pigment concentration of 0.2 mg m^{-3} (see text).

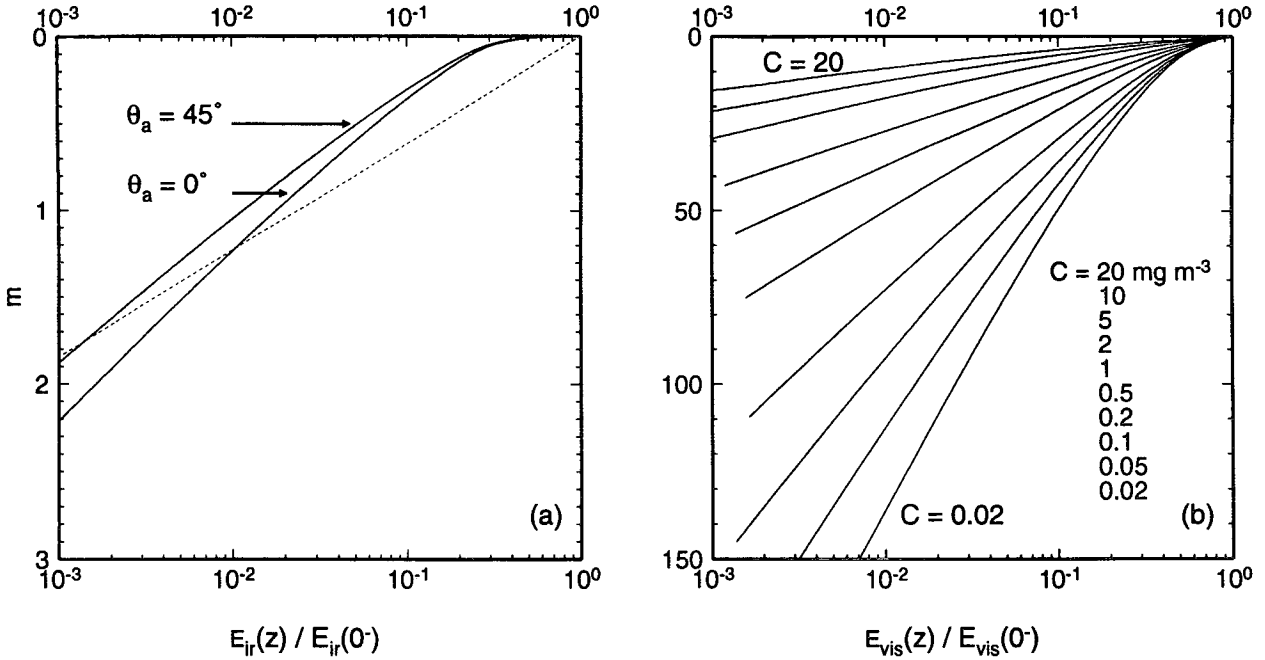

FIG. 2. Vertical profiles of downwelling irradiance normalized with respect to irradiance just below the surface (0^-). (a) For the near-IR solar radiation ($\lambda > 0.75$ μm) and a solar zenith angle (in air), θ_a of 0° and 45°; the dashed line represents Eq. (8). (b) For short wavelengths including UV radiation ($\lambda < 0.75$ μm) and various chlorophyll pigment concentrations (C, in mg m^{-3}) as indicated. Note that the vertical pigment profiles are assumed to be uniform (C = const) and that the radiation propagation is assumed to be independent from the illumination (solar angle) conditions (see text).

larger (e.g., see Hale and Querry 1973) that it seems advisable to separately consider two spectral ranges, below and above 0.75 μm. Below this limit and particularly in the blue–green domain, the sea water absorption is dependent on its algal content. Above this wavelength, additional absorption, if any, remains totally negligible in comparison to that of pure water. Thus, whatever the oceanic water turbidity, a single formulation of the heating rate associated with the IR absorption appears sufficient. The consequence of very high absorption is as follows: the in-water radiative field being dominated by absorption, scattering is inoperative in rearranging the light field and, in particular, in creating a significant upward radiant stream. In such a situation, the diffuse attenuation coefficient for net downwelling irradiance tends simply to reduce to the absorption along a slant path, hence

$$K_v = K_d = a/\cos\theta_w, \qquad (6)$$

where θ_w is the zenith angle of the refracted sun rays. By using the spectral composition of incident radiation combined with $a(\lambda)$, the absorption coefficients (for $\lambda > 0.75$ μm) adopted from Hale and Querry (1973; see also Table 1), the vertical profile of the whole IR radiation, $E_{IR}(Z)$, can be computed according to

$$E_{IR}(Z) = \int_{0.75}^{2.75} E_{IR}(Z, \lambda)d\lambda, \qquad (7a)$$

where

$$E_{IR}(Z, \lambda) = E_{IR}(0^-, \lambda)\exp[-K_d(\lambda)Z]. \qquad (7b)$$

Here, $K_d(\lambda)$ is given by Eq. (6), and E_{IR} (0^-, λ) is derived from E_{IR} (0^+, λ), as computed via the 5S model, by using the appropriate value of the Fresnel reflectance [Eq. (5)].

2) PARAMETERIZATION FOR THE INFRARED RADIATION PROPAGATION

It turns out that the long wavelength radiation attenuates quickly (Fig. 1) so that this energy is totally (99.9%) absorbed within the upper 2 meters (Fig. 2a). When the solar elevation angle decreases, the thickness of this IR-absorbing layer decreases as $\cos\theta_w$. Note that in this spectral range, the diffuse sky radiation is small compared to the direct sun radiation; therefore, the above approximate formulation [Eqs. (6) and (7)], which involves only the direct solar flux direction, can be safely adopted. By assuming a single exponential decay for $E_{IR}(Z)$, Eqs. (7a) and (7b) can be replaced by

$$E_{IR}(Z) = E_{IR}(0^-)\exp(-Z/0.267\cos\theta_w), \qquad (8)$$

where the attenuation length (0.267 m) is adjusted in such a way that, when the sun is at zenith, 99% of the IR radiation is absorbed within a layer extending down

to 1.23 m [as when using Eqs. (7a) and (7b)]. A single attenuation length for such polychromatic radiation obviously ignores, and cannot reproduce, the curvature of the vertical profile within the very top layer (Fig. 2a). Near-surface absorption is thus underestimated down to 20–30 cm and slightly overestimated deeper, even if the global heat deposition inside the upper 2-m deep layer is correctly estimated. This approximation is sufficient for practical applications, apart from those dealing with the specific question of the sea surface temperature as detected by satellite (especially in case of very calm seas).

3) Ultraviolet visible domain

The heat flux associated with penetrating solar irradiance and its dependence on the bio–optical state have been described in Morel (1988), but only for the radiation band between 400 and 700 nm. It is therefore necessary to account for the spectral domain 300–400 and 700–750 nm. The parameterization of the attenuation coefficient for downwelling irradiance rests upon the formalism previously used to express the nonlinear relationship between $K_d(\lambda)$ and the chlorophyll pigment concentration, C (Morel 1988):

$$K_d(\lambda) = K_w(\lambda) + \chi(\lambda)[C]^{e(\lambda)}. \quad (9)$$

Here $K_w(\lambda)$ represents the spectral value of the diffuse coefficient for optically pure water. In the range 400–700 nm the coefficients $\chi(\lambda)$ and the exponents $e(\lambda)$ were obtained from regression analyses performed on the log-transformed data [$K_d(\lambda)$ in m^{-1}, and C in mg Chl m^{-3}]. Reproduced from the above reference these three parameters (with $\Delta\lambda = 5$ nm) are given in Table 1, together with the new values, extrapolated as explained below.

The rationale when extrapolating the χ and e values is as follows. In the near IR it is simply assumed that the oceanic biogenous material is no longer absorbing beyond 750 nm; thus, χ is made regularly decreasing from 0.03 (its value at 700 nm) down to 0 (at 750 nm), whereas the value of the exponent is kept constant (0.60).

In the near-UV, measurements of the Chl-specific absorption $a^*(\lambda)$ for algae in culture have been frequently carried out down to 350 or 360 nm; $a^*(\lambda)$ is the spectral absorption coefficient of a pure algal suspension, after dividing by its chlorophyll content. The shape of the $a^*(\lambda)$ spectrum is a guideline to predict the spectral values of the Chl-specific attenuation coefficient for downwelling irradiance, denoted $k_c(\lambda)$. It has been shown (Morel 1988) that the $k_c(\lambda)$ and $a^*(\lambda)$ spectral shapes tend to coincide at high C values. In such eutrophic waters, the influence of associated biogenic (living and detrital) materials is reduced compared to that of living algae. In contrast, an inverse situation is observed in oligotrophic waters with very low C values. For such waters, the $k_c(\lambda)$ spectrum tends to resemble that of nonalgal materials; the maximum at 440 nm vanishes and is replaced by a featureless branch, weakly ascending toward shorter wavelengths (e.g., see Bricaud and Stramski 1990). The k_c coefficient being the derivative of K_d with respect to the pigment concentration, it is therefore expressed as

$$k_c(\lambda) = e(\lambda)\chi(\lambda)[C]^{e(\lambda)-1}. \quad (10)$$

With both these constraints, at very high and very low C values, it is possible to infer plausible values for $\chi(\lambda)$ and $e(\lambda)$ from 400 down to 350 nm. Below 350 nm, information is scarce, in particular about the existence of a quantitative link between the $K_d(\lambda)$ values and the pigment concentration. The only data available (Smith and Baker 1981; Baker and Smith 1982) have been tentatively used to constrain the extrapolation of the $\chi(\lambda)$ and $e(\lambda)$ parameters from 350 to 300 nm. The uncertainty in this extrapolation is of minor importance in the present problem, because this spectral domain provides less than 2% of the total radiant energy (the conclusion should be different as far as the ecological implications of the solar UV penetration would be concerned).

The entire set of $K_w(\lambda)$, $\chi(\lambda)$, and $e(\lambda)$ values within the interval 300–750 nm is provided in Table 1. With these values, the $K_d(\lambda)$ spectra can be computed through Eq. (9) for varying C values, ranging between 0.02 and 20 mg m^{-3} (Figs. 3a and 3b). The spectral values of the downwelling irradiance at some selected depths and when $C = 0.2$ mg m^{-3} are also displayed in Fig. 1.

The penetration of the UV and visible downwelling irradiance can be assessed by integrating with respect to wavelengths, in a way similar to that used for E_{IR} [Eq. (7a)]. The limits of the spectral range are 300 and 750 nm, and $K_d(\lambda)$, now depending on C, is expressed through Eq. (9). In relation with the local absorption [Eq. (1)], the downwelling irradiance must be corrected to account for the upwelling stream, no longer negligible for this spectral domain. The spectral values of reflectance, shown in Fig. 9 (see the appendix) as a function of the chlorophyll pigment concentration, have to be used to derive the net downward flux through $E_d(\lambda)[1 - R(\lambda)]$. Here, E_{vis}, which represents the flux for the entire UV–visible domain, is finally obtained as a function of depth through

$$E_{vis}(Z) = \int_{300}^{750} E_d(Z, \lambda)[1 - R(\lambda)]d\lambda, \quad (11a)$$

where

$$E_d(Z, \lambda) = E_d(0^-, \lambda)\exp[-K_d(\lambda)Z] \quad (11b)$$

and where K_d and R are independent of Z in these equations but do depend on C. Examples of vertical profiles of E_{vis} are provided in Fig. 2b. These computations are considered as "accurate" to the extent that the full set of parameters (91 spectral values of k_w, χ,

TABLE 1. For the range 400–700 nm the K_w, χ, and e values [Eq. (8)] are reproduced from Table 2 in Morel (1988); K_w is expressed as m^{-1}. In the 300–400 and 700–750 nm domains the K_w values are interpolated between those proposed by Smith and Baker (1981), and the additional χ and e values are selected as described in the text. For the 750–2600 nm domain, the values of the absorption coefficient, a, to be used in Eq. (6), are derived from the values of the imaginary part of the index of refraction, as given in Hale and Querry (1973).

λ (nm)	$K_w(\lambda)$ (m^{-1})	$\chi(\lambda)$	$e(\lambda)$	λ (nm)	$K_w(\lambda)$ (m^{-1})	$\chi(\lambda)$	$e(\lambda)$	λ (nm)	$a(\lambda)$ (m^{-1})
300	.154	.196	.889	530	0.052	.047	.670	775	2.400
305	.135	.191	.878	535	0.054	.045	.665	800	1.963
310	.116	.187	.867	540	0.057	.044	.660	825	2.772
315	.105	.183	.856	545	0.062	.043	.655	850	4.331
320	.094	.179	.845	550	0.064	.041	.650	875	5.615
325	.085	.174	.834	555	0.068	.040	.645	900	6.786
330	.076	.170	.823	560	0.072	.039	.640	925	14.401
335	.070	.166	.812	565	0.076	.038	.630	950	38.764
340	.064	.161	.801	570	0.081	.036	.623	975	44.857
345	.058	.157	.790	575	0.094	.034	.615	1000	36.317
350	.053	.153	.778	580	0.107	.033	.610	1200	103.568
355	.048	.149	.767	585	0.128	.033	.614	1400	1238.685
360	.044	.144	.756	590	0.157	.032	.618	1600	671.515
365	.040	.140	.737	595	0.200	.033	.622	1800	802.851
370	.035	.136	.720	600	0.253	.034	.626	2000	6911.504
375	.031	.131	.700	605	0.279	.035	.630	2200	1650.764
380	.027	.127	.685	610	0.296	.036	.634	2400	5005.604
385	.025	.123	.673	615	0.303	.038	.638	2600	15321.306
390	.023	.119	.670	620	0.310	.038	.642		
395	.022	.114	.668	625	0.315	.040	.647		
400	.021	.110	.668	630	0.320	.042	.653		
405	.020	.111	.672	635	0.325	.043	.658		
410	.020	.112	.680	640	0.330	.044	.663		
415	.019	.113	.687	645	0.340	.045	.667		
420	.018	.113	.693	650	0.350	.045	.672		
425	.018	.110	.701	655	0.370	.046	.677		
430	.017	.108	.707	660	0.405	.047	.682		
435	.017	.106	.708	665	0.418	.049	.687		
440	.017	.104	.707	670	0.430	.052	.695		
445	.017	.100	.704	675	0.440	.052	.697		
450	.017	.097	.701	680	0.450	.051	.693		
455	.017	.094	.699	685	0.470	.044	.665		
460	.017	.090	.700	690	0.500	.039	.640		
465	.017	.086	.703	695	0.550	.034	.620		
470	.018	.082	.703	700	0.650	.030	.600		
475	.018	.079	.703	705	0.742	.025	.600		
480	.019	.075	.703	710	0.834	.020	.600		
485	.020	.073	.704	715	1.002	.015	.600		
490	.022	.069	.702	720	1.170	.010	.600		
495	.024	.066	.700	725	1.485	.007	.600		
500	.027	.064	.700	730	1.800	.005	.600		
505	.032	.060	.695	735	2.090	.002	.600		
510	.038	.058	.690	740	2.380	.000	.600		
515	.045	.054	.685	745	2.420	.000	.600		
520	.049	.050	.680	750	2.470	.000	.600		
525	.051	.047	.675						

e, and R) are used. In reference to these accurately computed profiles, the next step is to develop a less computationally expensive parameterization, with, however, the capability of reproducing the main features of the profiles, as well as their dependency on the pigment content.

4) PARAMETERIZATION FOR THE VISIBLE RADIATION PROPAGATION

To simulate this propagation a bimodal exponential function is selected, as in Kraus (1972), but here restricted only to the near-UV–visible portion of the solar spectrum. The various vertical profiles $E_{vis}(Z)$, computed for various values of C (where C was kept constant along with depth), are separately fitted (least square roots method) on an equation of the form

$$E_{vis}(Z) = E_{vis}(0^-)[V_1 \exp(-Z/Z_1) + V_2 \exp(-Z/Z_2)], \quad (12)$$

where V_1 and V_2 (with $V_1 + V_2 \equiv 1$) represent partitioning factors and Z_1, Z_2 are the associated attenuation

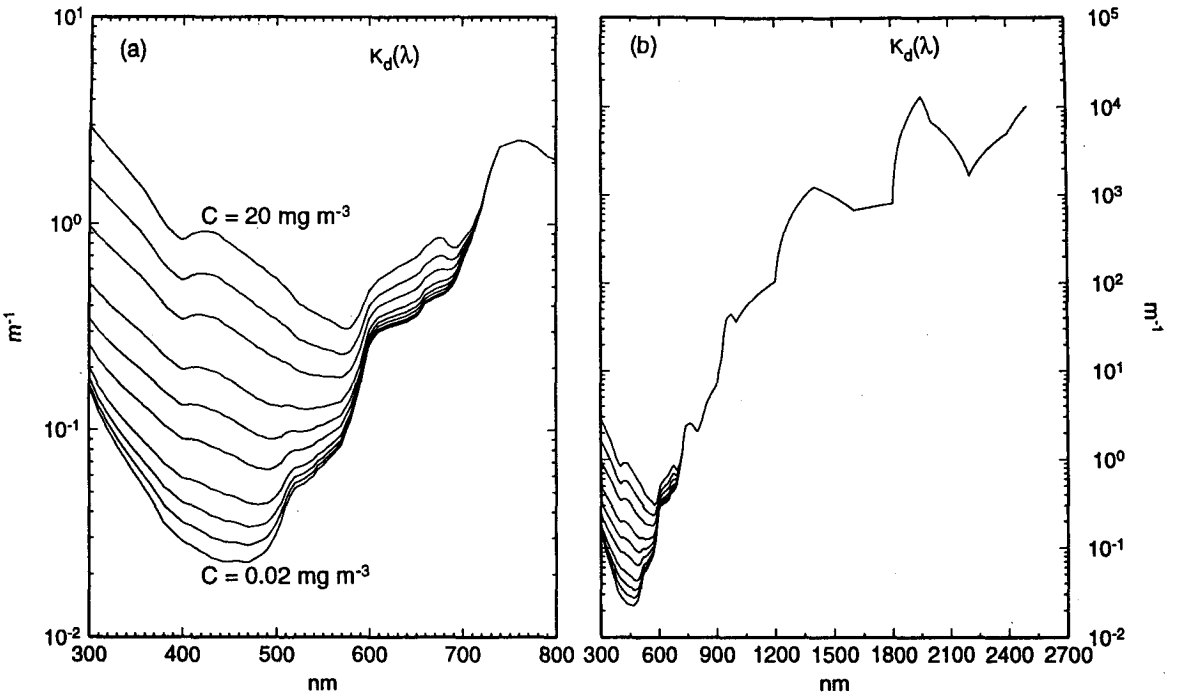

FIG. 3. Spectral values of the attenuation coefficient for downwelling irradiance computed for various pigment concentration values, as in Fig. 2, for (a) the 300–750 nm domain and (b) the full solar spectral domain up to 2.5 μm (the curves shown in panel *a* are included).

lengths. These four parameters are themselves functions of C, as shown in Figs. 4a (for V_1 and V_2) and 4b (for Z_1 and Z_2). The first term, and the first couple $V_1 - Z_1$, correspond to the longwave, less penetrating radiation, while absorption of the most penetrating radiation (shorter wavelengths) is represented by the second term and the couple $V_2 - Z_2$. As expected, Z_2 is markedly decreasing for increasing pigment concentration. The switch from blue to green ambiance in the in-water light field, which occurs around a hinge value of about 2 mg m^{-3} (see Fig. 12 in Morel 1988), entails a decrease in V_1 (and a correlative increase in V_2) beyond this value. The variations of these four parameters as functions of $\log_{10} C$ ($=X$) are conveniently described by polynomial expressions provided in Table 2 and used to construct the continuous curves in Figs. 4a and 4b.

In many parts of the ocean, and except when deep convection occurs, the algal biomass profile is vertically structured rather than uniform. Situations with deep chlorophyll maxima in oligotrophic stratified waters and situations with a near-surface maximum in eutrophic waters are extreme cases, between which the shape of the profile can evolve. In a statistical sense, this evolution is rather regular, as shown in Morel and Berthon (1989), and a parameterization has been proposed [Eq. (6) in this reference] that allows the pigment profile to be derived from C_{sat}, the pigment concentration within the upper layer, detectable by a remote sensor. The thickness of this layer is equal to the first "penetration depth" according to Gordon and McCluney (1975). These modeled pigment profiles, which include a Gaussian peak varying in magnitude and position, are used to derive the modified profiles. By again fitting these profiles on Eq. (12), new values for the four parameters appearing in Eq. (12) are obtained. They are also displayed in Figs. 4a and 4b as a function of C_{sat}. In terms of attenuation lengths (Z_1 and Z_2), the difference between the nonuniform and uniform situations is minute. For the partitioning factors (V_1 and V_2), the difference between the curves is reversing when C ($=C_{sat}$) exceeds 3 mg m^{-3}. The reason for this feature is to be found in the parameterization of the profiles. The broad Gaussian peak stays near the surface when the pigment value is above 3 mg m^{-3}. Below this value and when C is decreasing, the pigment maximum is deepening and increasingly developed. The usefulness of this modified set of V_1, V_2, Z_1, and Z_2 values will be discussed in the last part.

5. Heating rate profiles

The local heating rate can be computed either by operating the full spectral model, or, according to the purpose of the present work, by taking advantage of the spectral partitioning and simpler parameterizations [Eqs. (8) and (12)].

The full spectral model (considered hereafter as reference) consists of using the parameters in Table 1

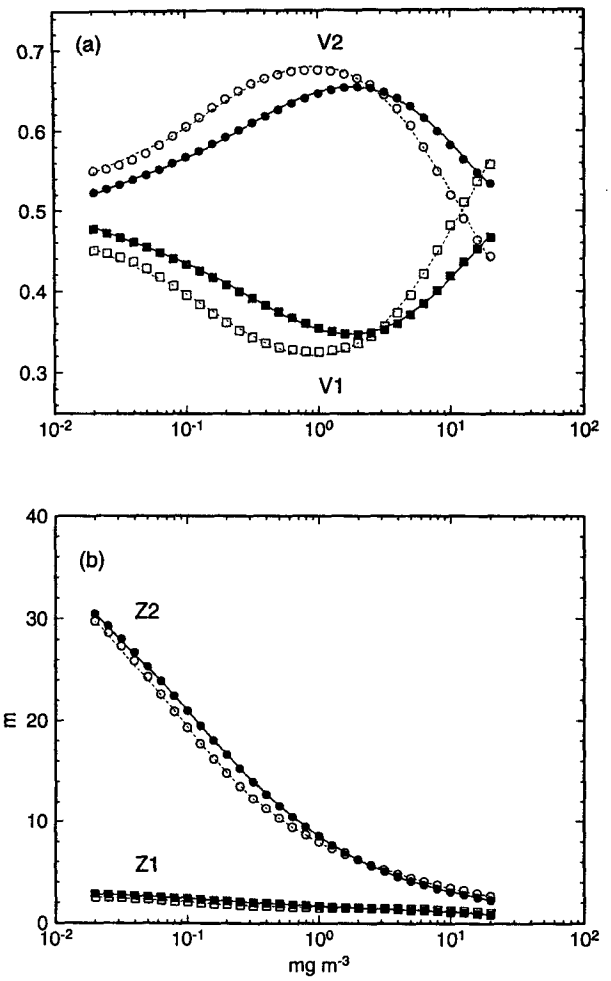

FIG. 4. (a) V_1 and V_2, and (b) Z_1 and Z_2 [in reference to Eq. (10)], as a function of chlorophyll concentration (log scale, units mg m^{-3}). Squares (V_1, Z_1) and circles (V_2, Z_2) are the results of the full spectral computation, for uniform pigment profiles (black symbols) or profiles including a Gaussian peak (open symbols). The continuous curves represent the polynomial adjustment (Table 2) for uniform (solid curve) or nonuniform (dashed curve) pigment profiles.

together with the IR absorption coefficients of Hale and Querry (1973) to obtain at each wavelength the vertical profiles of the downward irradiance $E_d(\lambda, Z)$ or of the net downward irradiance $[E_d(\lambda, Z) - E_u(\lambda, Z)]$, according to whether the IR or visible domains are considered. Then by differentiating with respect to depth [Eq. (1)] and using the appropriate depth increment, the amount of absorbed energy per 5-nm-wide waveband is obtained. After summing over the whole spectrum, E_{abs} is obtained at any depth. The corresponding vertical profiles are shown in Fig. 5a. For these computations the spectral distribution of the incident radiation is as in Fig. 1 and its integral is used for normalizing. As an example, the corresponding heating rates are also shown by assuming that the amount of radiant energy introduced under the surface is 10 MJ m^{-2} (recall that the daily insolation varies between 0 and more than 30 MJ m^{-2}).

The simplified computation consists of merging the two expressions developed before for the IR domain and the UV–visible domain, so that

$$E_{tot}(Z)/E_{tot}(0^-) = F_{IR}\,e^{-Z/0.267\cos\theta_w} + F_{vis}[V_1 e^{-Z/Z_1} + V_2 e^{-Z/Z_2}], \quad (13)$$

where $E_{tot}(0^-)$ and $E_{tot}(Z)$ are the total net downwelling irradiances (0.3–2.5 μm), just below the surface and at the depth Z, respectively, and where F_{IR} and F_{vis} (with $F_{IR} + F_{vis} \equiv 1$) represent the fractions of total irradiance above or below 0.75 μm; namely,

$$F_{IR} = E_{IR}(0^-)/E_{tot}(0^-)$$

$$F_{vis} = E_{vis}(0^-)/E_{tot}(0^-).$$

According to Eq. (1), E_{abs} is analytically expressed as the derivative of Eq. (13):

$$E_{abs}(Z)/E(0^-) = (F_{IR}/0.267\cos\theta_w)e^{-Z/0.267\cos\theta_w} + F_{vis}[(V_1/Z_1)e^{-Z/Z_1} + (V_2/Z_2)e^{-Z/Z_2}]. \quad (14)$$

The results are displayed in Fig. 5b for the same waters as in Fig. 5a. The profiles derived from Eq. (14) contain some "footprints" of the three exponential terms that successively predominate in the decay function, while the full spectral model (5a) generates more regular patterns. The other difference is the higher local E_{abs} values at the initial depth (Z = 10 cm) when Eq. (14) is used. The reason can be clearly identified in Fig. 2a; the energy absorbed between 0 and 10 cm is largely underestimated by using the exponential function and remains to be absorbed deeper. Such nuances (between Figs. 5a and 5b), mainly occurring within the first meter, are insignificant from a practical viewpoint. More important is the general agreement between the profiles in Figs. 5a and 5b. The spreading of the profiles, induced by the varying bio-optical state of the water, appears below 2 or 3 m and increases with

TABLE 2. Tabulated values of the coefficients appearing in the polynomials form $Y = a_0 + a_1X + a_2X^2 + a_3X^3 + a_4X^4 + a_5X^5$, where X is $\log^{10}(C)$ and Y is V_1, V_2, Z_1, or Z_2. The upper and lower parts of the table are for uniform and nonuniform pigment profiles, respectively (see text and Figs. 4a, b).

	a_0	a_1	a_2	a_3	a_4	a_5
V_1	0.353	−0.047	0.083	0.047	−0.011	−0.009
V_2	0.647	0.047	−0.083	−0.047	0.011	0.009
Z_1	1.662	−0.605	0.128	−0.033	−0.051	−0.004
Z_2	8.541	−8.924	4.020	−0.077	−0.536	0.055
V_1	0.321	0.008	0.132	0.038	−0.017	−0.007
V_2	0.679	−0.008	−0.132	−0.038	0.017	0.007
Z_1	1.540	−0.197	0.166	−0.252	−0.055	0.042
Z_2	7.925	−6.644	3.662	−1.815	−0.218	0.502

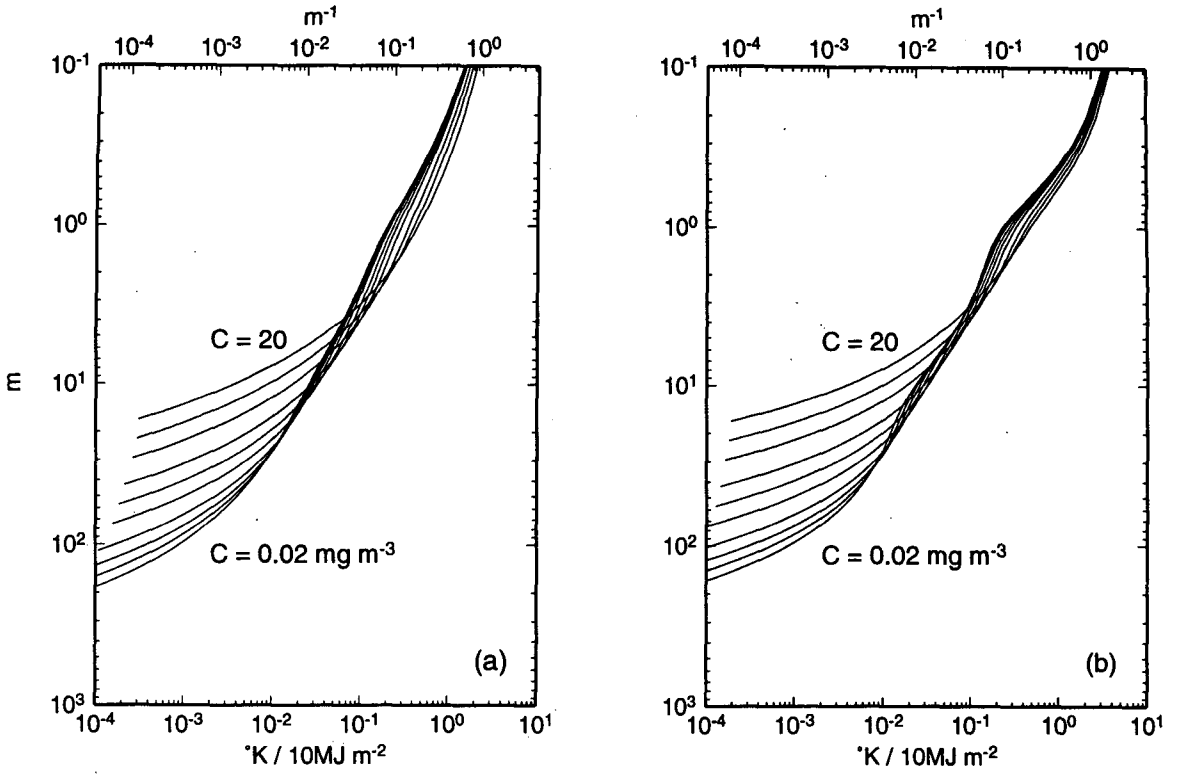

FIG. 5. Vertical profiles of the locally absorbed energy E_{abs} and of the correlative local heating. Absorbed energy E_{abs} (W m^{-3}) is normalized with respect to the incident energy just below the surface (W m^{-2}) so that units are m^{-1}. Local heating (K) is computed when assuming an incident irradiation of 10 MJ m^{-2} (second abcissae scale). (a) Results of the full spectral model; (b) results provided by the proposed parameterization resulting in the analytical expression [Eq. (14)]. Pigment values are as in Fig. 2.

depth. At 15 m for instance, the heating rate in very clear, oligotrophic waters is about 100 times higher than in green eutrophic waters. Similar heat deposition occurs at about 100 m, instead of 10 m, in extremely blue and green waters, respectively. In the former case, a significant heating may therefore take place below the mixed layer (the depth of the upper-ocean mixed layer being frequently less than 100 m).

An effective attenuation coefficient for the (total) net downward irradiance, K_{tot}, can be derived for any depth and bio-optical state. According to its operational definition [Eq. (2)], an analytical expression giving $K_{tot}(Z)$ is straightforwardly obtained as being the quotient of Eq. (14) by Eq. (13). Such an analytical expression, however, produces the same kind of artifactual curvatures as in Fig. 5b. The smoother K_{tot} profiles, starting at 1 cm (Fig. 6) are computed using the full spectral approach. As expected, the values higher than 1 m^{-1} are restricted to the very top layer ($\sim$10 cm). The K_{tot} values decrease and become diversified deeper. At the bottom of the curves, limited when the residual flux is reduced to about 10^{-3} of its initial value at surface, K_{tot} tends toward a limiting value, which is that of the most penetrating wavelength characteristic of the water in question, and of its pigment content (see also Fig. 15 in Morel 1988, drawn only for the 400–700-nm domain).

6. Practical use of the present model

The present model, developed for oceanic case 1 waters, allows the vertical profile of the solar radiation absorption and heating rate to be predicted as a function of the bio-optical state. The radiant energy flux at the ocean surface is presumably known (either measured or modeled) with the spatial and temporal resolutions adapted to the problem envisaged, as, for instance, the diurnal structure and evolution of the upper ocean at a given location, or the daily or weekly thermal trend within a given zone. A detailed discussion of the environmental conditions that determine the amount and spectral composition of the incident radiant flux is beyond the scope of the present study. Some specific aspects, however, dealing with the particular parameters introduced in the present modeling need to be examined.

a. Partitioning the solar spectrum

Splitting this spectrum into two domains, resulting in two independent terms inside Eq. (13), provides a

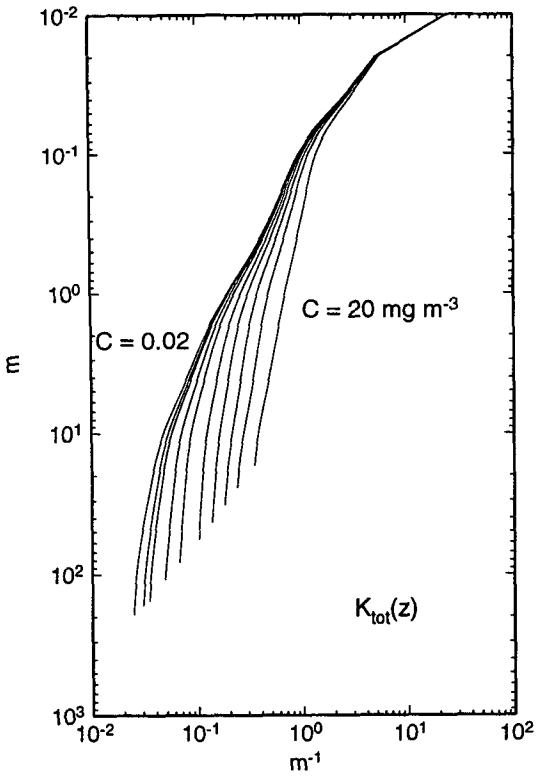

FIG. 6. Local value (as a function of depth) of the effective attenuation coefficient for net downwelling irradiance when all radiations contained within the whole solar spectrum are considered (K_{tot}). Pigment values are as in Fig. 2.

useful flexibility when operating this equation to the extent that the atmospheric and oceanographic input parameters are disconnected. The fractions F_{IR} and F_{vis} must be selected according to the illumination conditions and also the time scale envisaged.

For clear skies, F_{IR} and F_{vis} are mainly dependent upon the solar zenith angle and the water vapor content; to a lesser extent, these fractions also depend on the ozone and aerosol contents (Baker and Frouin 1987). Atmospheric models or analytical formulations (Bird and Riordan 1986; Frouin et al. 1989) are available to compute these fractions from climatological or satellite-derived data relative to the needed atmospheric parameters. Since UV and visible radiation are merged (in F_{vis}), and also because the lower limit of IR is more commonly set at 0.7 μm, instead of 0.75 μm, as adopted here, typical values of F_{vis} and F_{IR} must be provided. For clear skies F_{vis} ranges between 0.54 and 0.57 for a large variation of sun angle and atmospheric conditions (see Fig. 7). For cloudy skies, the transmitted light is bluer, whereas water vapor and liquid water absorption may considerably reduce the IR radiation able to reach the ocean surface. The resulting increase in F_{vis} can be estimated by using the semiempirical model of Nann and Riordan (1991), in conjunction with cloud transmittance estimated from satellite measurements of albedo (Dedieu et al. 1987). As a first approximation, a typical mean value of 0.60 could be given to F_{vis} for overcast skies.

b. Using the parameterized expression for absorption

It is assumed at this stage that the values for the fractions F_{IR} and F_{vis} (as well as θ_w) are known, or that averaged values have been adopted in adequacy with the problem and the temporal resolution aimed at. Given a certain amount of incident energy above the surface, $E(0^+)$, corrected for the ocean albedo [Eq. (5) and appendix], the amount of absorbed energy at any depth, $E_{abs}(Z)$, can be computed for any oceanic water provided that the chlorophyll pigment content in the upper layers is known. With this information and by using the polynomial expressions in Table 2, the four parameters, V_1, V_2, Z_1, and Z_2, are determined. Then Eq. (14) can be solved straightforwardly for any Z, or as well, integrated over a given depth interval (for instance, between zero and the depth of the mixed layer).

7. Discussion and conclusion

Some remaining questions about the approximations and choices have not yet been discussed and are examined below. The importance of nonheating processes

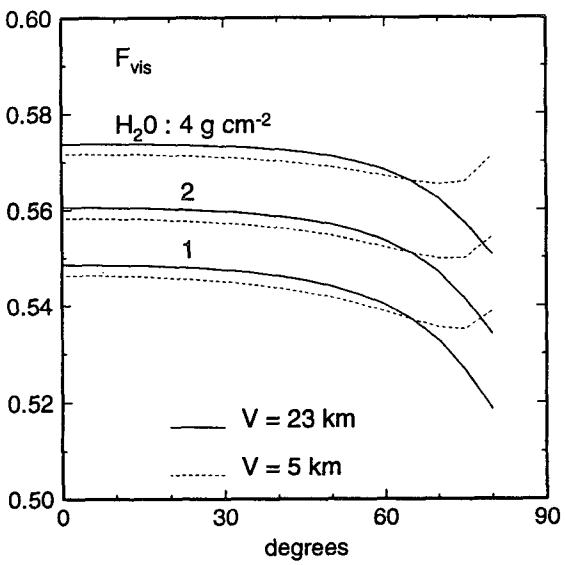

FIG. 7. Fraction of the total solar radiation at the sea surface, which corresponds only to the spectral domain with $\lambda < 0.75$ μm (F_{vis}, see text), plotted as a function of solar zenith angle. Maritime aerosol loads corresponding to moderately hazy and clear atmosphere (visibility of 5 or 23 km) are considered, and also three values of the water vapor content (1, 2, 4 g cm^{-2}, from bottom to top). Computations were made using the radiative transfer model of Tanré et al. (1979, 1990) and are also used for Fig. A1.

following radiation absorption also deserves some discussion.

1) The nonuniform pigment profiles lead (Fig. 4) to a slightly different set of parameters (lower part of Table 2). If a figure is drawn using these modified parameters, the difference between these profiles and those in Fig. 5b is hardly discernible. At the most, E_{abs} can be enhanced by 15% (when $C = 0.02$ mg m^{-3}), at the level of the deep chlorophyll maximum; this enhancement, however, occurs at a depth where the residual radiant energy is so low (about 1% of the initial energy) that this process is without noticeable impact. The nonuniform pigment profiles admittedly represent statistically averaged profiles; thus, it cannot be excluded that more intense deep maxima may on occasion exist, with a stronger impact on the local heating rate [as hypothesized and analyzed by Lewis et al. (1983)] and possibly on the vertical convective process.

2) Opticists familiar with the radiative transfer in the ocean may argue that some approximations still remain in the full spectral model. In the visible part of the spectrum, the reflectance $R(\lambda)$ is not strictly a constant with respect to depth, even in a homogeneous water body. Near the surface $R(\lambda)$ is influenced by the sun angle (Gordon 1989; Morel and Gentili 1991). In the same fashion, $K_d(\lambda)$ is also slightly depth dependent, particularly in the upper layer. In this layer, however, the heating process results primarily from the absorption of IR radiation and the corresponding attenuation coefficients actually have been made dependent upon the solar elevation [Eq. (6), Fig. 2a]. For the visible radiation this dependence is ignored [Eq. (9), Fig. 2b]. This approximation is practically valid because (i) the heating resulting from absorption of the visible radiation within the top few centimeters is unimportant compared to that of near-IR and (ii) when the absorption of visible radiation becomes important in relative proportion, that is, at deeper levels where IR has already disappeared, the variations in K_d and R tend to become minute.

3) The diffuse attenuation for downwelling irradiance at 490 nm is a property of the upper ocean that can be derived from space observation (Austin and Petzold 1981). Its use has often been suggested to predict the heating rate of the upper layer. The structures of the algorithms providing $K_d(490)$ and the pigment concentration, C, actually are similar. In essence, these two quantities are not independent and are rather redundant in the algorithmic scheme developed for the Coastal Zone Color Scanner and case 1 waters (see in Gordon and Morel 1983). Here, C has been selected as the relevant bio-optical index because, thanks to previous studies, a complete spectral information about the optical properties of a water body can be associated with its chlorophyll pigment content. Second, in contrast to $K(490)$, C is routinely determined at sea, sometimes continuously monitored along transects, so that the present modeling can also apply in the case of field measurements.

4) It has been previously (section 3) mentioned that the fate of absorbed energy is not exclusively heating. Inelastic Raman scattering by water molecules is another pathway. The reemitted light, however, shifted toward longer wavelengths, is instantly absorbed locally. This molecular process ultimately does not modify the absorption process. Living algal cells absorb visible light, a small fraction of which is reemitted around 685 nm via chlorophyll fluorescence and then efficiently absorbed. The conclusion for this process is as for Raman emission. Another fraction is converted into heat because the yield of the photosynthetic machinery is limited. Last, a fraction is stored as chemical energy into the organic compounds resulting from photosynthesis and subsequent reactions. It has already been shown (Morel 1988, Fig. 18) that the ratio of such stored energy to available radiation at the surface remains very small (a few percent in the "best" eutrophic conditions). In addition, this chemical energy is transformed to heat, at least partly, within the same layers due to consumption and oxydation of the organic matter. Therefore this pathway, of prominent importance in biology and biogeochemistry, is completely negligible in the heat deposition process within the upper ocean.

If a detailed description of the solar radiation absorption within an oceanic water body can be accurately reached by using a full spectral model, at the cost of summing more than 100 exponential functions, it is presently shown that the proposed formulation, which includes only three exponential terms, can keep the essential features, with a gain in computation time by more than one order of magnitude. This formulation applies for about 98% of the World Ocean waters (case 1 waters) but is not valid for coastal (sediment- or yellow substance–dominated) case 2 waters. The information concerning the chlorophyll pigment content of the open ocean, expected on a routine basis from future ocean color sensors, can readily be introduced in any physical model with a minimum of computational effort, even on a pixel-by-pixel basis.

Acknowledgments. We are very thankful to Bernard Gentili for computing assistance and help with figure preparation. We also gratefully acknowledge the support of the European Space Agency (OT/MM/612 to A. Morel).

APPENDIX

Diffuse Reflectance and Fresnel (Specular) Reflectance of the Sea

a. The Fresnel reflectance at the air–sea interface

The specular reflection is the predominant process in forming the albedo of the sea surface [Eq. (5)]. The sum ($\rho_F + \rho_D$) of the Fresnel reflectance and diffuse

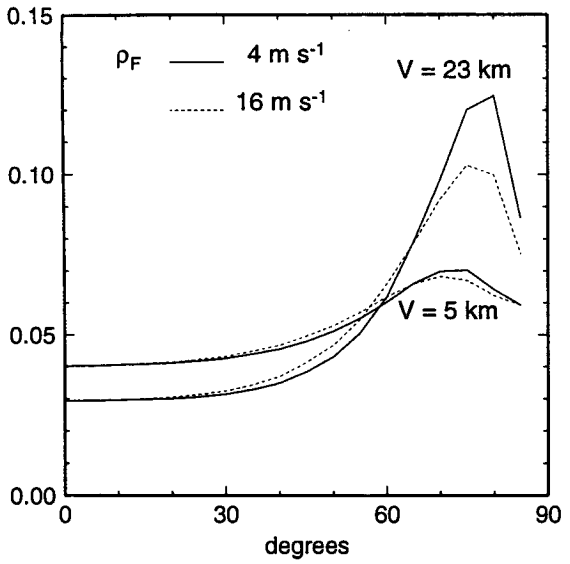

FIG. A1. Bulk Fresnel reflectance for the total solar radiation at the air–sea interface, ρ_F, as a function of zenith sun angle and for two visibilities (5 and 23 km) and two wind velocities (4 and 16 m s^{-1}).

reflectance may vary from about 3% for high sun elevation angle and clear skies, to more than 30%, for low solar elevation (Payne 1972). In contrast, the sole ρ_D term is at most 0.7% (see below).

In Payne (1972) the albedo values are tabulated as a function of sun elevation angle and atmospheric transmittance, and climatological values are also provided. For overcast skies the typical ρ_F value generally adopted is 6.6%, in correspondence with an isotropic sky radiance distribution. Roughening of the surface by wind modifies the reflectance value (Austin 1974; Preisendorfer and Mobley 1986), and in particular depresses the large reflectances to be expected at high latitude, with low sun elevation. The uncertainty in this term crucially limits the accuracy when estimating the amount of solar energy introduced within, and then absorbed by, the ocean. Compared to this uncertainty in ρ_F, the consideration of ρ_D could appear useless.

Improved estimates of ρ_F are nevertheless at reach, by systematically operating atmospheric models, and an example is provided in Fig. A1. The atmospheric model of Tanré et al. (1979, 1990) allows estimates of the (sky) diffuse and (sun) direct irradiance components to be separately made. For the former component a constant reflectance (6.6%) is used, whereas a sun angle- and wind-dependent reflectance (Austin 1974) is applied to the direct component. The water vapor content is without influence on the results, contrary to the aerosol load, which determines the relative proportions of direct and diffuse radiations and therefore the bulk ρ_F values. There is no particular problem in producing, through several available atmospheric models, tabulated ρ_F values, as a function of sun angle and atmospheric conditions, in as much as such values would be needed in a specific problem.

b. *Diffuse reflectance*

The irradiance ratio or reflectance, R, is involved when dealing with this fraction (ρ_F) of the incident flux that is backscattered to the atmosphere and thus is not captured by the ocean [Eq. (5)], and also when assessing the net downward flux [Eq. (11)].

With the parameters listed in Table 1 and by following the same iterative scheme as previously developed (Morel 1988), the spectral values of the reflectance, $R(\lambda)$, can be computed for the UV–visible domain as a function of the chlorophyll pigment concentration C. The results are displayed in Fig. A2 (which is an extension of Fig. 13 in Morel 1988). They do not include inelastic or transspectral scattering processes (Raman or fluorescence emissions). There is no particular problem in using these (tabulated) data when using Eq. (11). It is readily seen that the corrective effect of R, practically negligible (<1%) when $\lambda > 600$ nm, can be significant in the violet–blue part of the spectrum, in particular for low-chlorophyll waters.

Due to internal reflection, including complete reflection of upwelling radiances with incidence angle exceeding the critical angle (~48°), the upwelling radiative flux just below the interface (0^-) is only partially transmitted through the interface. It must be multiplied by a transmittance of about 0.52 (Austin 1974) so that

$$R(0^+, \lambda) = 0.52R(0^-, \lambda).$$

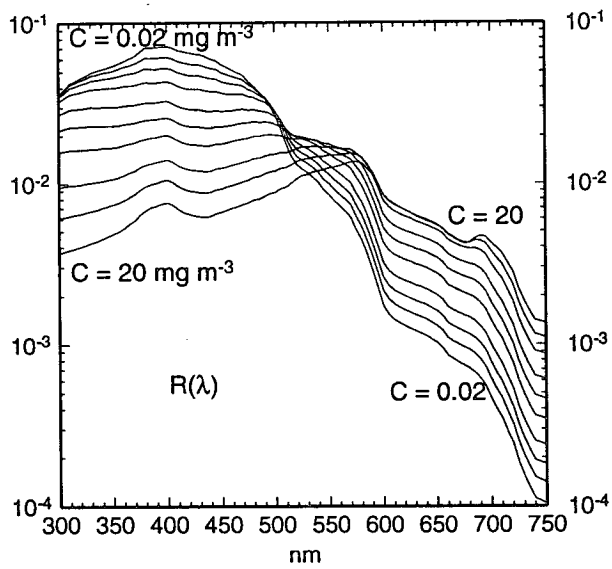

FIG. A2. Spectral values of the reflectance in the domain 300–750 nm, and for various chlorophyll pigment concentrations as in Fig. 2.

TABLE 3. Bulk diffuse reflectance of the ocean [ρ_D in percent, Eq. (15)], as a function of the chlorophyll pigment concentration (C). The upper limit of the wavelength range is either 0.75 or 2.5 μm (note that the spectral values of reflectance are zero in the 0.75–2.5 μm domain).

Spectral range (μm)	C (mg m^{-3})									
	0.02	0.05	0.1	0.2	0.5	1	2	5	10	20
0.3–0.75	1.21	1.13	1.05	0.96	0.83	0.74	0.65	0.55	0.47	0.38
0.3–2.5	0.68	0.64	0.59	0.54	0.47	0.42	0.37	0.31	0.26	0.22

The term ρ_D is an average value of $R(0^+, \lambda)$ over the whole spectrum and also must account for the spectral composition of the incident radiation

$$\rho_D = \int_{0.3}^{\lambda\,\max} R(0^+, \lambda) \cdot E_d(0^+, \lambda) d\lambda \Big/ \int_{0.3}^{\lambda\,\max} E(0^+, \lambda) d\lambda. \quad (15)$$

By using, as weighting function, a spectral composition of incident radiation similar to that shown in Fig. 1, the mean diffuse reflectance ρ_D can be computed as a function of the chlorophyll pigment concentration and for the spectral domain up to $\lambda_{max} = 0.75$ μm (UV–visible), or for the entire domain ($\lambda_{max} = 2.5$ μm); note that R is always zero when $\lambda > 0.75$ μm. These values (Table 3), would be slightly dependent on the sea state through the transmittance factor, which increases from 0.515 up to 0.537 when the wind speed increases from 0 to 16 m s^{-1} (Austin 1974).

REFERENCES

Austin, R. W., 1974: The remote sensing of spectral radiance from below the ocean surface. *Optical Aspects of Oceanography,* N. G. Jerlov and E. Steemann Nielsen, Eds., Academic, 317–344.

——, and T. J. Petzold, 1981: The determination of the diffuse attenuation coefficient of sea water using the Coastal Zone Color Scanner. *Oceanography from Space,* J. R. F. Gower, Ed., Plenum Press, 239–256.

Baker, K. S., and R. C. Smith, 1982: Bio-optical classification and model of natural waters: 2. *Limnol. Oceanogr.,* **27,** 500–509.

——, and R. Frouin, 1987: Relation between photosynthetically available radiation and total insolation at the ocean surface under clear skies. *Limnol. Oceanogr.,* **32,** 1370–1377.

Bird, R. E., and C. Riordan, 1986: Simple solar spectral model for direct and diffuse irradiance on horizontal and tilted planes at the earth's surface for cloudiness atmospheres. *J. Climate Appl. Meteor.,* **25,** 87–97.

Bishop, J. K., and W. B. Rossow, 1991: Spatial and temporal variability of global surface solar irradiance. *J. Geophys. Res.,* **96,** 16 839–16 858.

Bricaud, A., and D. Stramski, 1990: Spectral absorption coefficients of living phytoplankton and non-algal biogenous matter: A comparison between the Peru upwelling area and Sargasso Sea. *Limnol. Oceanogr.,* **35,** 562–582.

Dedieu, G., P. Y. Deschamps, and Y. H. Kerr, 1987: Satellite estimation of solar irradiance at the surface of the earth and of surface albedo using a physical model applied to meteosat data. *J. Climate Appl. Meteorol.,* **26,** 79–87.

Denman, K. L., 1973: A time-dependent model of the upper ocean. *J. Phys. Oceanogr.,* **3,** 173–184.

Frouin, R., D. W. Lingner, C. Gautier, K. S. Baker, and R. C. Smith, 1989: A simple analytical formula to compute clear sky total and photosynthetically available solar irradiance at the ocean surface. *J. Geophys. Res.,* **94,** 9731–9742.

Gautier, C., G. Diak, and S. Masse, 1980: A simple physical model to estimate incident solar radiation at the surface from GOES satellite data. *J. Appl. Meteorol.,* **19,** 1005–1012.

Gordon, H. R., 1989: Dependence of the diffuse reflectance of natural waters on the sun angle. *Limnol. Oceanogr.,* **34,** 1484–1489.

——, and W. R. McCluney, 1975: Estimation of the depth of sunlight penetration in the sea for remote sensing. *Appl. Opt.,* **14,** 413–416.

——, and A. Morel, 1983: Remote assessment of ocean color for interpretation of satellite visible imagery, a review. *Lecture Notes on Coastal and Estuarine Studies,* Springer-Verlag, 114 pp.

Hale, G. M., and M. R. Querry, 1973: Optical constants of water in the 200 nm to 200 μm wavelength region. *Appl. Opt.,* **12,** 555–563.

Iqbal, M., 1983: *An Introduction to Solar Radiation.* Academic Press, 390 pp.

Jerlov, N. G., 1976: *Marine Optics.* Elsevier, 231 pp.

Kirk, J. T. O., 1988: Solar heating of water bodies as influenced by their inherent optical properties. *J. Geophys. Res.,* **93,** 10 897–10 908.

Kraus, E. B., 1972: *Atmosphere–Ocean Interaction.* Oxford University Press, 275 pp.

Lewis, M. R., J. J. Cullen, and T. Platt, 1983: Phytoplankton and thermal structure in the upper ocean: Consequences of nonuniformity in chlorophyll profile. *J. Geophys. Res.,* **88,** 2565–2570.

——, M. E. Carr, G. C. Feldman, W. Esaias, and C. McClain, 1990: Influence of penetrating solar radiation on the heat budget of the equatorial Pacific Ocean. *Nature,* **347,** 543–545.

Morel, A., 1988: Optical modeling of the upper ocean in relation to its biogenous matter content (Case I waters). *J. Geophys. Res.,* **93,** 10 749–10 768.

——, and L. Prieur, 1977: Analysis of variations in ocean color. *Limnol. Oceanogr.,* **22,** 709–722.

——, and R. C. Smith, 1983: Terminology and units in optical oceanography. *Mar. Geodesy,* **5,** 335–349.

——, and J. F. Berthon, 1989: Surface pigments, algal biomass profiles and potential production of the euphotic layer: Relationships reinvestigated in view of remote sensing applications. *Limnol. Oceanogr.,* **34,** 1547–1564.

——, and B. Gentili, 1991: Diffuse reflectance of oceanic waters: Its dependence on sun angle as influenced by the molecular scattering contribution. *Appl. Opt.,* **30,** 4427–4438.

Nann, S., and C. Riordan, 1991: Solar spectral irradiance under clear and cloudy skies: Measurements and semiempirical model. *J. Appl. Meteor.,* **30,** 447–462.

Neckel, H., and D. Labs, 1984: The solar radiation between 3300 and 12 500 A. *Solar Phys.,* **90,** 205–258.

Paulson, C. A., and J. J. Simpson, 1977: Irradiance measurements in the upper ocean. *J. Phys. Oceanogr.,* **7,** 953–956.

Payne, R. E., 1972: Albedo of the sea surface. *J. Atmos. Sci.,* **29,** 959–970.

Preisendorfer, R. W., and C. D. Mobley, 1986: Albedos and glitter patterns of a wind-roughened sea surface. *J. Phys. Oceanogr.,* **16,** 1293–1316.

Raschke, E., 1975: Numerical studies of solar heating of an ocean model. *Deep-Sea Res.,* **22,** 659–665.

Rossow, W. B., and R. A. Schiffer, 1991: ISCCP cloud data products. *Bull. Amer. Meteor. Soc.*, **72,** 2–20.

Simonot, J. Y., and H. Le Treut, 1986: A climatological field of mean optical properties of the World Ocean. *J. Geophys. Res.*, **91,** 6642–6646.

Simpson, J. J., and T. D. Dickey, 1981: The relationship between downward irradiance and upper ocean structure. *J. Phys. Oceanogr.*, **11,** 309–323.

Smith, R. C., and K. S. Baker, 1978: The bio–optical state of ocean waters and remote sensing. *Limnol. Oceanogr.*, **23,** 247–259.

——, and ——, 1981: Optical properties of the clearest natural waters. *Appl. Opt.*, **20,** 177–184.

Stephens, G. L., 1978: Radiation profiles in extended water vapor clouds. 2: Parameterization schemes. *J. Atmos. Sci.*, **35,** 2123–2132.

Tanré, D., M. Herman, P. Y. Deschamps, and A. de Leffe, 1979: Atmospheric modeling for space measurements of ground reflectances, including bidirectional properties. *Appl. Opt.*, **18,** 3587–3594.

——, C. Deroo, P. Duhaut, M. Herman, J. J. Morcrette, J. Perbos, and P. Y. Deschamps, 1990: Description of a computer code to simulate the satellite signal in the solar spectrum: the 5S code. *Int. J. Remote Sens.*, **11,** 659–668.

Woods, J. D., 1980: Diurnal and seasonal variation of convection in the wind-mixed layer of the ocean. *Quart. J. Roy. Meteor. Soc.*, **106,** 379–394.

Zaneveld, J. R. V., and R. W. Spinrad, 1980: An arctangent model of irradiance in the sea. *J. Geophys. Res.*, **85,** 4919–4922.

——, J. C. Kitchen, and H. Pak, 1981: The influence of optical water type on the heating rate of a constant depth mixed layer. *J. Geophys. Res.*, **86,** 6426–6428.